Equilibrium Unfolding of the Dimeric SAM Domain of MAPKKK Ste11 from the Budding Yeast: Role of the Interfacial Residues in Structural Stability and Binding†

Anirban Bhunia,‡ Prerna N. Domadia,‡ Xiaolong Xu,§ Richard Gingras,§ Feng Ni,§ and Surajit Bhattacharjya*,‡

Biomolecular NMR and Drug Discovery Laboratory, Division of Structural and Computational Biology, School of Biological Sciences, Nanyang Technological University, Singapore 637551, and Biotechnology Research Institute, 6100 Royalmount Avenue, Montreal, Quebec, Canada H4P2R2

Received September 25, 2007; Revised Manuscript Received November 12, 2007

ABSTRACT: The sterile α motifs or SAM domains are small (∼70 amino acids) protein−protein interaction modules that are involved in diverse functions ranging from cell signaling, transcription regulation, and scaffolding. The Ste11 protein kinase in the mitogen-activated protein kinase (MAPK) signaling cascades of the budding yeast is regulated by a SAM domain located at the N-terminus of the full-length protein. The Ste11 SAM domain forms a symmetrical dimeric structure with an interface stabilized presumably by hydrophobic and ionic interactions. Here, we investigated urea-induced unfolding, using NMR and other optical spectroscopic methods, of the dimeric Ste11 SAM domain and two of the variants, namely, L57R and L60R, each containing a point mutation at the interfacial region. Our results demonstrate that the residue-specific or global unfolding of the Ste11 SAM is highly cooperative without any evidence for folded monomeric or partially folded species. However, replacement of hydrophobic residues with basic residues in the interface caused considerable changes in the stability and folding of the Ste11 SAM domain. The native dimeric structure of the L60R mutant protein is severely affected as indicated by a high propensity toward aggregation. On the other hand, the L57R mutant, although retaining the native structure, shows a dramatic decrease in the conformational stability as revealed by urea-induced denaturation and amide proton exchange studies. Furthermore, isothermal titration calorimetry and intrinsic tryptophan fluorescence experiments demonstrate that the L57R interacts with the cognate SAM domain from Ste50 with reduced affinity, while the L60R protein is devoid of any detectable binding activity. These results demonstrate that the interfacial residues of the dimeric SAM domain of Ste11 are critically involved in its structural stability and binding to the Ste50 SAM domain.

The sterile α motifs or SAM[1] domains are multifunctional protein modules that are essential in a variety of regulatory processes ranging from cell signaling, transcription repression, and synaptic scaffolding to translational control (*1*−*4*). SAM domains were first identified from multiple sequence alignment studies in Ste11 and Ste50 proteins from MAPK signaling cascades of the budding yeast along with a few other proteins involved in development of the fruit fly (*5*, *6*). The functions of most SAM domains are manifested by their roles in mediating specific protein−protein interactions (*1*−*4*). In particular, SAM domains form heterocomplexes with other SAM domains (*7*−*10*) or with other proteins such as the PDZ and SH2 domains (*11*−*13*). Many SAM domains, e.g., those from ph, TEL, and Yan, have been shown to regulate gene transcriptions through extensive self-associations (*14*−*16*). Very recently, a SAM domain from the Shank protein has been described as the "master scaffolder" due to its role in organizing multiprotein complexes in the neuronal synapses (*3*, *17*). Apart from protein−protein interactions, SAM domains of the post-transcriptional regulator Smg protein from *Drosophila melanogaster* and the Vts1 protein of yeast have been shown to bind specific sequences of RNA (*18*−*20*). Three-dimensional structures, determined by NMR spectroscopy and X-ray crystallography, of several SAM domains exhibit a protein fold consisting of five helices of different lengths (*4*, *7*, *14*−*17*, *21*−*28*), which have been established as responsible for diverse functions of different SAM domains. Despite the functional importance of the conserved SAM fold, there is still a lack of understanding of the structural stability and folding properties of these domains.

We have been investigating the structures and interactions of SAM domains and other proteins from the MAPK signaling pathways of the budding yeast (*29*−*31*). In these signaling cascades, a MAPKKK Ste11 contains a SAM domain at its N-terminal region (residues D37−R104) that interacts with the SAM domain of an adaptor protein, Ste50

† This work is funded by the Academic Research Fund (Grant RG66/06) of Nanyang Technological University and by the Genomics and Health Initiative (GHI) program of the National Research Council of Canada, sponsored by the Government of Canada (NRCC Publication No. 49535). A.B. is supported by a grant from the A*star BMRC (06/01/22/19/446), Singapore.

* To whom correspondence should be addressed. E-mail: surajit@ntu.edu.sg. Fax: +65-6791-3856. Phone: +65-6316-7997.

‡ Nanyang Technological University.

§ Biotechnology Research Institute.

[1] Abbreviations: SAM, sterile α motif; NMR, nuclear magnetic resonance; CD, circular dichroism; HSQC, heteronuclear single quantum coherence; MAPKKK, mitogen-activated protein kinase kinase kinase; MAPK, mitogen-activated protein kinase; ITC, isothermal titration calorimetry; H/D exchange, hydrogen/deuterium exchange.

10.1021/bi701941z CCC: $40.75
Published on Web 12/20/2007

(*32*, *33*). The interaction between Ste11 and Ste50, mediated by their SAM domains, is required for the activation of Ste11 kinase (*32*, *33*). Previously, we have demonstrated that the Ste11 SAM domain forms a symmetrical dimer in solution with a canonical SAM-fold of five helices (*29*). In the solution structure, the dimeric interface seems to be stabilized by intimate contacts among several hydrophobic residues and ionic interactions between two helices, helix 4 and helix 5, at the C-terminus of the molecule (*29*). However, it was not immediately clear whether the residues at the dimeric interface play any role in the stability and assembly of the Ste11 SAM domain.

In this work, we examined urea-induced unfolding of the dimeric Ste11 SAM domain and two of its interfacial mutant proteins. Our results demonstrate that the native dimeric structure of Ste11 SAM undergoes cooperative unfolding without any detectable folded monomeric or partially folded intermediate states. The urea- mediated unfolding of the Ste11 SAM dimer appears to be complete only at a urea concentration of ~6 M. The L57R mutant although retains a nativelike folded structure; however, there is a significant loss in conformational stability. On the other hand, the L60R mutant has lost the specific dimeric structure and is characterized by a marked tendency toward aggregation. In interaction studies with the Ste50 SAM domain, the L57R shows a considerable reduction in binding affinity as compared to the native protein, whereas the L60R mutant does not show any detectable binding. Unfolding and interaction studies, presented here, clearly suggest that hydrophobic residues at the dimeric interface play dominant role(s) in maintaining the stability and structural integrity of the Ste11 SAM domain and in conferring binding to the cognate SAM domain from the Ste50 protein.

MATERIALS AND METHODS

Site-Directed Mutagenesis and Protein Expression and Purification. Ste11 SAM (D37−R104) (*29*) and Ste50 SAM (M27−D108) domains from *Saccharomyces cerevisiae* were subcloned into the pET14b vector with a thrombin cleavable N-terminal His_6 tag and overexpressed in *Escherichia coli* BL21 (DE3) cells. The amino acid sequence of the Ste11 SAM was numbered as D1−R68. A QuickChange mutagenesis (Stratagene) kit was used to make the two mutants L57R and L60R in the Ste11 SAM domain. Both mutations were confirmed by DNA sequencing. The expressed proteins were purified as described previously (*29*). Briefly, overexpressing *E. coli* cells were grown at 37 °C in either LB or M9 medium with [^{15}N]ammonium chloride (Cambridge Isotope Laboratories) and induced at an OD_{600} of 0.6−0.7 with 0.3 mM IPTG. After incubation for 6−12 h at 15 °C for protein production, the cells were centrifuged and resuspended in 20 mM Tris−hydrochloride buffer, pH 8.0. The cell solution was lysed by sonication, and the supernatant was applied to a nickel−NTA column for His-tag-based purification (Qiagen). The protein-loaded column had been extensively washed with appropriate buffers to remove weakly bound proteins. Strongly bound target proteins were eluted from the resins with 500 mM imidazole. The purified proteins were extensively dialyzed against 10 mM sodium phosphate buffer, containing 150 mM NaCl and 20 mM β-mercaptoethanol, at pH 5.8 for the native Ste11 SAM and mutant proteins L57R and L60R. For the interaction studies with the Ste50 SAM domain, using ITC and fluorescence, protein samples were prepared in the above buffer with a pH of 6.8.

NMR Spectroscopy. All NMR experiments were performed at 15 °C on a Bruker DRX 600 MHz spectrometer equipped with an actively shielded cryoprobe or on a Bruker Avance-800 spectrometer. NMR data were processed using the NMRPipe and NMRDraw (*34*, *35*) suite and analyzed by Sparky (T. D. Goddard and D. G. Kneller, University of California, San Francisco). All the chemical shifts were indirectly referenced to DSS. Denaturation experiments were performed by adding aliquots of a 9 M stock solution of urea, prepared in 10 mM sodium phosphate buffer, 150 mM NaCl, and 20 mM β-mercaptoethanol, pH 5.8, into an NMR tube containing either the ^{15}N-labeled native Ste11 SAM at 0.4 mM or the ^{15}N-labeled L57R mutant protein at the same concentration. The samples were allowed to equilibrate for 20 min before two-dimensional ^{1}H−^{15}N HSQC spectra were recorded. The reduction in the intensity of HSQC cross-peaks as a function of the denaturant concentration was fitted to the following equation (*36*):

$$Y_{obs} = \frac{(\alpha N + \beta N[\mathrm{D}])}{1 + \exp\{-[m([\mathrm{D}] - Cm)/RT]\}}$$

where Y_{obs} represents the intensity of an HSQC peak, α and β are the intercept and slope of the pre- and postunfolding regimes, respectively, m is the slope at the midpoint of the unfolding transition, [D] is the concentration of the denaturant, C_m is the denaturant concentration at the midpoint of the transition, and RT is 0.57 kcal mol^{-1}.

Hydrogen/Deuterium Exchange. To study amide proton exchange, lyophilized Ste11 SAM and the L57R mutant protein were dissolved in a D_2O buffer of 10 mM sodium phosphate, 150 mM NaCl, and 20 mM β-mercaptoethanol at pH 5.8. A series of two-dimensional ^{1}H−^{15}N HSQC spectra were acquired within an interval of 30 min. Hydrogen exchange rates (k_{ex}) were fitted to a single-exponential decay equation. The protection factors were determined from a ratio of calculated intrinsic exchange rates of the amide protons of proteins (*37*) and the experimentally measured exchange rates.

Circular Dichroism Measurements. CD experiments were performed using a Chirascan circular dichroism spectrophotometer (Applied Photophysics Ltd., U.K.). The far-UV CD spectra of the three protein samples, the native Ste11 SAM, L57R, and L60R, were collected from 190 to 230 nm at 20 °C after correction of the baseline. CD spectral scans were taken three times and averaged using a 0.01 cm path length sandwich cuvette. Data were collected at a spectral bandwidth of 1 nm and step size of 0.4 nm to improve the signal-to-noise ratio. The sample concentrations were adjusted to 10 μM in 10 mM sodium phosphate, 150 mM sodium chloride, and 20 mM β-mercaptoethanol at pH 5.8. For urea-induced unfolding studies the samples were equilibrated with increasing concentrations of urea (0.2−7 M) for 15 min. CD spectra were plotted as a function of molar ellipticity.

Fluorescence Measurements: The intrinsic tryptophan fluorescence emission spectra of the Ste50 SAM domain were acquired using a Cary Eclipse fluorescence spectrophotometer (Varian, Inc.) equipped with dual monochromators. The native Ste11 SAM and its interfacial mutant L57R and L60R proteins were titrated with increasing concentra-

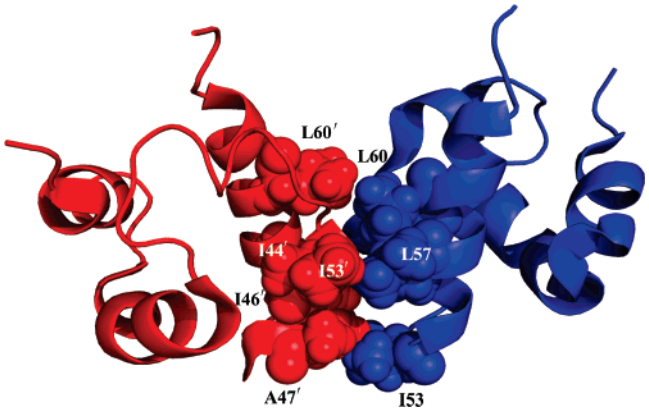

FIGURE 1: Space-filling representation of nonpolar packing interactions at the dimer interface of the Ste11 SAM domain. The helices are represented by ribbons. Two structural subunits are distinguished by different colors.

tions ranging from 0.2 to 5.0 μM to a fixed concentration, 1 μM, of the Ste50 SAM domain in a buffer containing 10 mM sodium phosphate, 150 mM sodium chloride, and 20 mM β-mercaptoethanol, pH 6.8. Measurements were made in the 300−400 nm range in a 0.1 cm path length quartz cuvette by exciting the samples at 280 nm. The band-passes for excitation and emission were set to 5 nm.

Isothermal Calorimetric Titration. Isothermal calorimetric titrations were performed on a VP-ITC microcalorimeter (Micro Cal Inc., Northampton, MA). A 10 μM concentration of Ste50 SAM in 10 mM sodium phosphate, 150 mM sodium chloride, and 20 mM β-mercaptoethanol, pH 6.8, was loaded into the sample cell (volume ~1.4 mL), and the reference cell was filled with the same buffer. In an individual ITC run, the native Ste11 SAM and the mutant proteins were loaded into the injectant at 10-fold higher concentrations (120 μM) than Ste50 SAM. A typical calorimetric reaction was carried out by titrating 20 injections of 5 μL aliquots of the native SAM or mutants into the sample cell at an interval of 5 min. The reaction cell was stirred continuously at 300 rpm at 20 °C. The heats of dilution, arising from the addition of native Ste11 SAM or the mutant proteins, were subtracted from the resultant isothermal titration profiles and further integrated using MicroCal Origin 5.0. The equilibrium association constant (K_a) and thermodynamic parameters were obtained by fitting the binding profile using a single-site binding model.

Size Exclusion Chromatography. Samples of Ste11 SAM and the L60R mutant were loaded onto a Hiload 16/60 Superdex 75 10/300 GL analytical column with the AKTA FPLC UPC-900 system (GE Healthcare UK Ltd., England). Prior to loading, the protein samples were dialyzed against 10 mM sodium phosphate buffer containing 150 mM sodium chloride and 20 mM β-mercaptoethanol, pH 5.8. The FPLC column was equilibrated with the same buffer, and the samples were eluted at a flow rate of 0.5 mL/min and detected spectrophotometrically at 276 nm.

RESULTS

Selection of Residues for Mutation. Figure 1 shows intersubunit interactions among hydrophobic residues located at the interface of the dimeric Ste11 SAM domain. The structural organization of the interface is sustained by packing of hydrophobic residues in the first half of helix 5 (residues I53−S65) from one subunit and helix 4′ (residues K42′−A47′) of the other subunit. We chose residues from helix 5 for mutation; they also have predominant occurrences at the interfacial regions of other oligomeric SAM domains including those of Eph B2 and Eph A4 (*4*, *24*, *25*). Among the three nonpolar interfacial residues in helix 5, the centrally located L57 makes a number of van der Waals contacts with residues I44′ and I46′ from helix 4′, whereas residue L60 is uniquely packed with L60′ from the other subunit (Figure 1). The solution structure of the Ste11 SAM domain also revealed an asymmetric charge distribution whereby the interfacial region is rich in positively charged residues (*29*). On this basis, we have assumed that replacement of hydrophobic residues from helix 5 with positively charged amino acids may destabilize the interfacial region of the Ste11 SAM domain by charge/charge repulsion.

Unfolding of the Dimeric Ste11 SAM Domain. Figure 2 summarizes urea-induced unfolding of the native Ste11 SAM as assessed by $^1H-^{15}N$ HSQC experiments and far-UV CD spectroscopy. A series of $^1H-^{15}N$ HSQC spectra of the Ste11 SAM domain were collected with increasing concentrations, ranging from 0.5 to 7 M, of urea (Figure 2A). In these experiments, we observed a reduction in intensity of the HSQC cross-peaks of the native dimer as a function of the urea concentration. The attenuation of the cross-peak intensity appears to be conspicuous only at urea concentrations above 2.0 M. The $^1H-^{15}N$ HSQC spectra of the Ste11 SAM, obtained at 5.0−5.5 M urea concentrations, are further characterized by the appearance of new resonances around 8.0−8.5 ppm in the amide proton region (Figure 2A). At these urea concentrations, HSQC cross-peaks from the folded dimeric structure are also clearly visible (Figure 2A), implying that the native and the unfolded states are in slow exchange at the NMR time scale. At a urea concentration of 6.0 M, the Ste11 SAM domain attains a largely unfolded state, since the HSQC spectrum contains sharper cross-peaks with a dramatic reduction in chemical shift dispersion, i.e., ~1.0 ppm, of the amide proton resonances (Figure 2A). The equilibrium unfolding of the Ste11 SAM domain obtained from the diminution of the HSQC cross-peak intensity is further analyzed by the two-state unfolding transition (see the Materials and Methods). A close superposition of the transition curves of residues corresponding to different regions of the molecule suggests that the dimeric structure apparently unfolds without any detectable population of stable intermediate states (Figure 2B). Moreover, a very similar C_m value for almost all the residues indicates a highly cooperative denaturation transition (Figure 2C). Unfolding of the Ste11 SAM has also been monitored by far-UV CD spectra at various concentrations of urea. Figure 2D represents reduction in the folded population of the Ste11 SAM, as deduced from the decrease in ellipticity (θ_M) at the 222 nm band of the CD spectra, with increasing concentrations of denaturant. The global unfolding of the dimeric Ste11 SAM appears to also be highly cooperative, revealed from the CD studies, with a midpoint of denaturation at a ~4 M urea concentration (Figure 2D). Collectively, these results demonstrate that the native dimeric structure of the Ste11 SAM domain is quite stable and completely unfolds only at a high urea concentration of 6 M. The unfolding transition is highly cooperative and occurs without any folded or partially folded stable structural states.

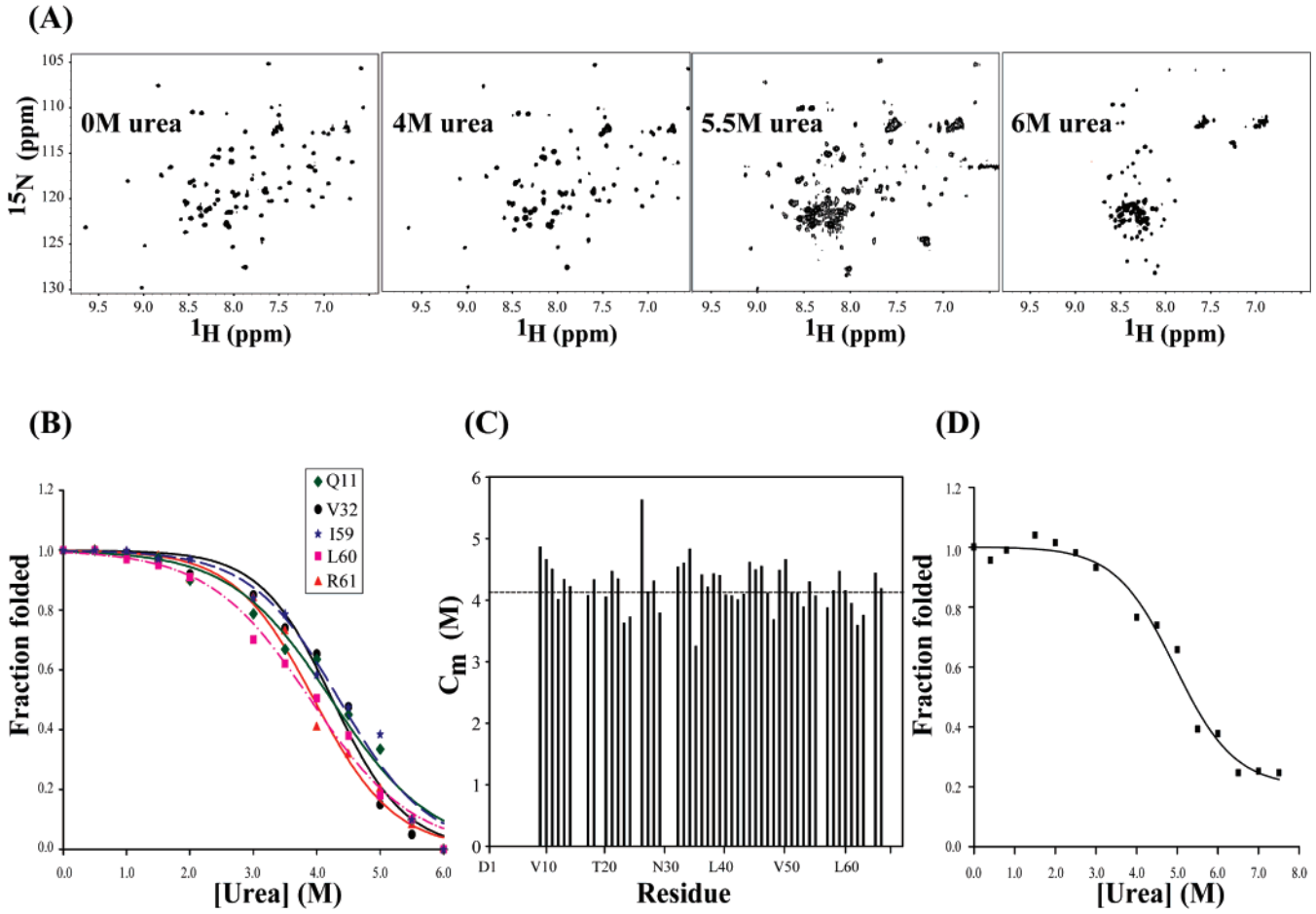

FIGURE 2: (A) Equilibrium unfolding of the ^{15}N-labeled Ste11 SAM domain as a function of increasing concentrations of urea by two-dimensional ^{1}H−^{15}N HSQC spectra. HSQC experiments were carried out at a protein concentration of 0.4 mM in 10 mM sodium phosphate buffer, 150 mM NaCl, and 20 mM β-mercaptoethanol, pH 5.8. (B) Change in the native folded population of the dimeric Ste11 SAM with increasing concentrations of urea of some representative resonances encompassing the N- and C-termini of the molecule. The reduction in the native population was estimated from the intensity of the HSCQ cross-peaks and normalized relative to the native-state spectrum. (C) Bar diagram delineating the concentration of urea at the midpoint (C_m) of the unfolding transition as a function of the residue of the native Ste11 SAM domain. The dashed line indicates an average C_m value of the Ste11 SAM domain. (D) Unfolding transition of the native dimeric Ste11 SAM as a function of increasing urea concentrations measured using far-UV CD spectra. The loss of native folded population was estimated from the ellipticity (θ_m) value obtained at 222 nm at different urea concentrations and normalized relative to the ellipticity at 222 nm observed without any denaturant. CD spectra were recorded using a sample concentration of 10 μM in 10 mM sodium phosphate buffer, 150 mM sodium chloride, and 20 mM β-mercaptoethanol, pH 5.8, at 15 °C.

Conformational Stabilities of the Interfacial Mutants L57R and L60R. The global folding of the two interface mutant proteins L57 and L60R was found to be very different (Figure 3). Figure 3A shows an overlay of the ^{1}H−^{15}N HSQC spectra of the native Ste11 SAM and L57R. Clearly, the mutant protein is well folded as suggested by the well-dispersed chemical shifts of the amide and nitrogen atoms. Almost all the HSQC cross-peaks of L57R could be assigned on the basis of resonance assignments of the native Ste11 SAM domain indicating that the L57R mutant retains a nativelike dimeric structure. Furthermore, the measurement of the hydrodynamic radius, using pulse-field gradient NMR, suggested that L57R retains the dimeric association (data not shown). On the other hand, the ^{1}H−^{15}N HSQC spectrum of the L60R is characterized by the presence of only a few cross-peaks (Figure 3B), demonstrating a dramatic change in the conformation of the mutant protein. Figure 3C compares the far-UV CD spectra of the two mutants L57R and L60R along with that of the native Ste11 SAM domain. Analogous to the native Ste11 SAM, both the mutant proteins L57R and L60R possess nativelike helical secondary structures. On the other hand, the oligomerization property of the L60R mutant is quite different, as its elution profile on size-exclusion chromatography was considerably broad with a much lower elution volume as compared to that of the native protein (Figure 3D). A sharp elution peak can be seen for the native dimeric form of the Ste11 SAM domain with some minor high molecular weight species appearing at lower elution volumes. It is noteworthy that the native Ste11 SAM domain also has an intrinsic tendency toward self-association over a prolonged period of time (*30*). These observations demonstrate that the interfacial mutant L60R must undergo extensive self-associations, resulting in the formation of high molecular weight soluble aggregates. The aggregated forms of L60R are rich in helical structures as suggested by the far-UV CD spectra (Figure 3C). Consequently, observation of a few cross-peaks in the HSQC spectrum of L60R (Figure 3B) appears to be an outcome of extremely broad resonances of the high molecular weight and aggregated species. The unfolding of the helical structures of L60R was also examined by far-UV CD spectra as a function of the urea concentration. The aggregated protein turns out to be

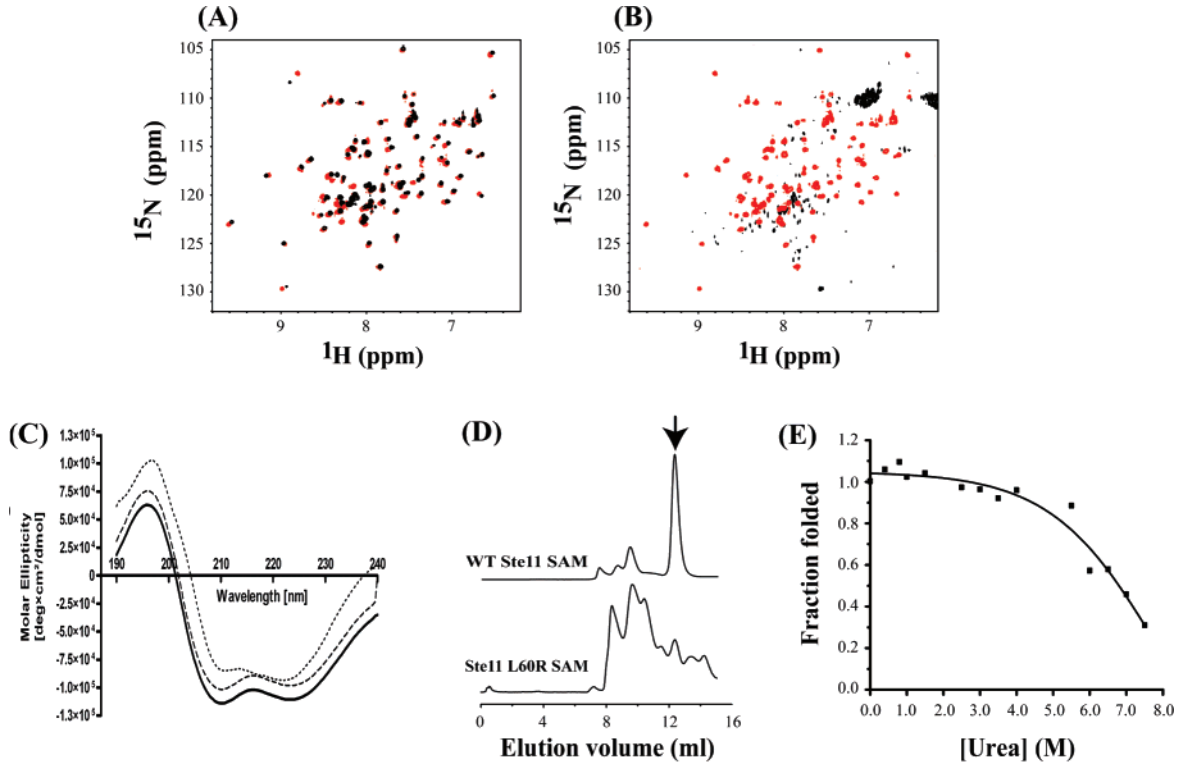

FIGURE 3: (A) Overlay of ^{1}H−^{15}N HSQC spectra of the native Ste11 SAM dimer (in red) and the L57R mutant protein (in black). (B) Overlay of ^{1}H−^{15}N HSQC spectra of the native Ste11 SAM dimer (in red) and the L60R mutant (in black). The HSQC spectrum was obtained at a protein concentration of 0.4 mM in 10 mM sodium phosphate buffer, 150 mM sodium chloride, and 20 mM β-mercaptoethanol, pH 5.8, at 15 °C. (C) Far-UV CD spectra of the native Ste11 SAM (—), L57R (···), and L60R (---). CD spectra were recorded using a sample concentration of 10 μM in 10 mM sodium phosphate buffer (pH 5.8), 150 mM sodium chloride, and 20 mM β-mercaptoethanol at 15 °C. (D) Size-exclusion chromatographic profiles of the native Ste11 SAM and L60R. A Superdex-75 column was equilibrated with 10 mM sodium phosphate buffer, pH 5.8, containing 150 mM NaCl and 20 mM β-mercaptoethanol. Samples (10 μM) in the same buffer were loaded and eluted at a flow rate of 0.5 mL/min. The peak shown by an arrow indicates the elution of the native dimeric Ste11 SAM domain. (E) Unfolding transition of the L60R mutant protein as a function of the urea concentration measured using far-UV CD spectra. The loss of the helical structure was estimated from the ellipticity (θ_m) value obtained at 222 nm at different urea concentrations and normalized relative to the ellipticity at 222 nm observed without any denaturant. CD spectra were recorded using a sample concentration of 10 μM in 10 mM sodium phosphate buffer (pH 5.8), 150 mM sodium chloride, and 20 mM β-mercaptoethanol at 15 °C.

extremely stable, since considerable secondary structures are observed even at 6.0 M or higher concentrations of the denaturant (Figure 3E).

The conformational stability of the L57R mutant was further examined by urea-dependent unfolding and H/D exchange studies (Figure 4). Figure 4A shows ^{1}H−^{15}N HSQC spectra of L57R at various concentrations of urea. The urea-induced unfolding of L57R is characterized by a decrease in intensity of the HSQC cross-peaks with increasing concentrations of denaturants akin to the native Ste11 SAM domain (Figure 2A). However, inspection of these HSQC spectra demonstrates a facile unfolding of the L57R mutant over the native Ste11 SAM. Very clearly, an apparently unfolded state of the L57R is achieved at a urea concentration of 5.5 M, as indicated by the loss of dispersion of the chemical shifts of the amide proton and nitrogen resonances (Figure 4A). By contrast, an overall unfolded state of the native Ste11 SAM domain was found only at urea concentrations of 6.0 M or above (Figure 2A). A close examination of the HSQC spectra of L57R reveals the appearance of unfolded species even at significantly lower concentrations of urea, e.g., 2.0 and 4.0 M, as indicated by overlapping HSQC cross-peaks at 8.0−8.5 ppm along the ^{1}H dimension (Figure 4A). Figure 4B shows representative ^{1}H−^{15}N HSQC spectra of the native Ste11 SAM and L57R obtained in D_2O buffer solution, pH 5.8, after 30 and 120 min of exchange. Many backbone amide protons of the native Ste11 SAM domain were found to be exchanging slowly as compared to those of the L57R mutant protein (Figure 4B). Indeed, all of the backbone amide protons of the L57R were replaced by solvent deuterium within 2.5 h of exchange (data not shown). Figure 4C enumerates the protection factor of amide protons of the native Ste11 SAM and the L57R mutant. Since most of the amide protons of the L57R undergo a fast H/D exchange, we were able to estimate the protection factors only for 11 amino acid residues. Significantly lower protection factors were observed for most of the residues throughout the primary amino acid sequence of the L57R mutant, suggesting an overall destabilization of the nativelike conformation (Figure 4C). Taken together, these results demonstrate that the interactions at the dimer interface of the Ste11 SAM domain are highly essential for its conformational stability and correct folding.

Interactions of L57R and L60R with the Ste50 SAM Domain. The binding activity of the native Ste11 SAM domain and two mutants, L57R and L60R, with the Ste50 SAM domain were examined by ITC (Figure 5) and intrinsic tryptophan fluorescence studies (Figure 6). Figure 5 demonstrates representative ITC thermograms of the interactions whereby aliquots of either the native Ste11 SAM domain (panel A) or the mutant proteins L57R (panel B) and L60R (panel C) were individually titrated into the sample cell

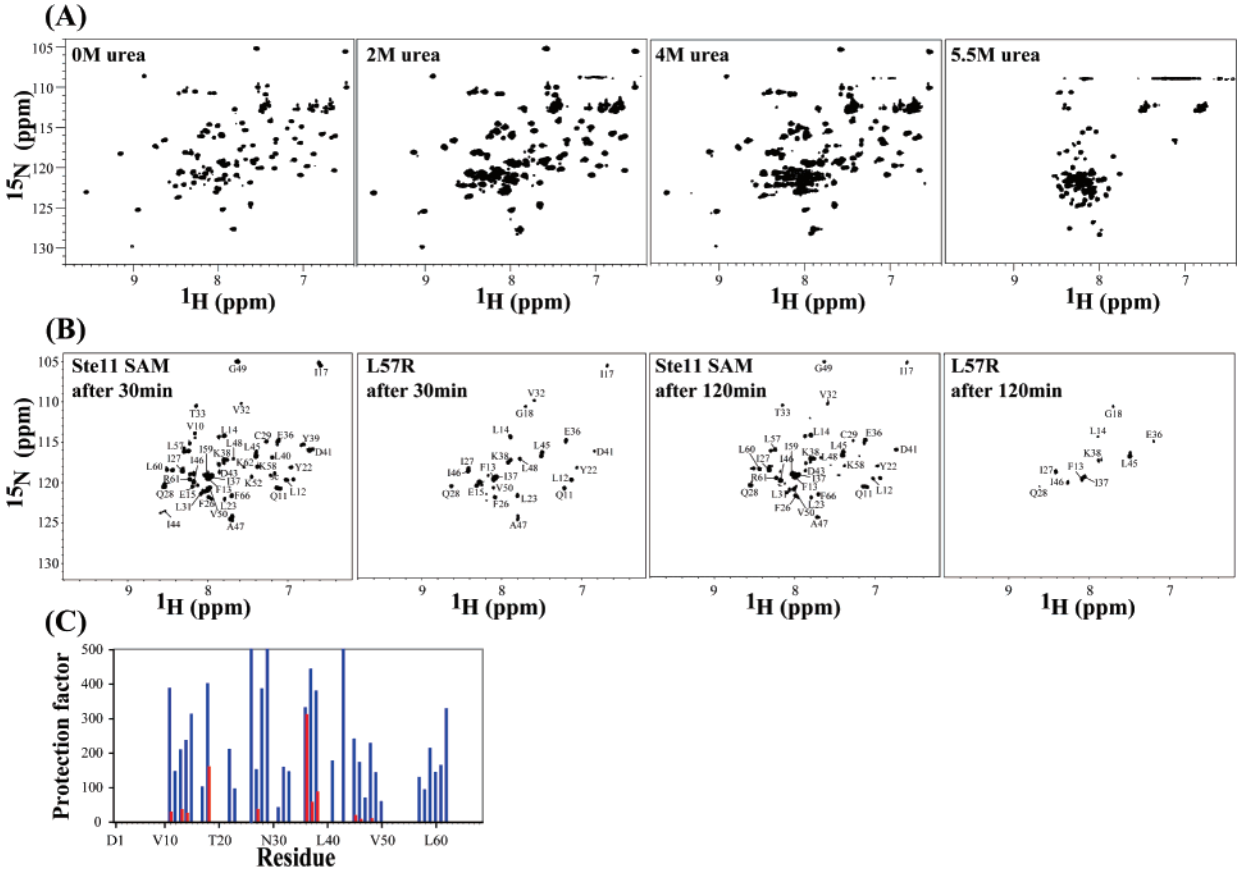

FIGURE 4: (A) $^{1}H-^{15}N$ HSQC spectra of the L57R mutant as a function of increasing concentrations of urea. HSQC experiments were carried out at a protein concentration of 0.4 mM in 10 mM sodium phosphate buffer, 150 mM NaCl, and 20 mM β-mercaptoethanol, pH 5.8, 15 °C. (B) Representative $^{1}H-^{15}N$ HSQC spectra of the native Ste11 SAM and L57R mutant showing amide proton exchange, after 30 and 120 min, against solvent D_2O. Samples were prepared by dissolving lyophilized powder in a D_2O buffer of 10 mM sodium phosphate, pH 5.8, containing 150 mM NaCl and 20 mM β-mercaptoethanol. The protein concentrations for H/D exchange studies were fixed at 0.5 mM. (C) Bar diagram showing the distribution of the protection factor of the amide protons of the native Ste11 SAM (in blue) and the L57R (in red).

containing a fixed concentration of the Ste50 SAM domain. Both the native Ste11 SAM and the L57R mutant were found to be interacting with the cognate Ste50 SAM domain as suggested by the release or absorption of heat in the ITC experiments (Figure 5A,B). On the other hand, titrating the L60R mutant into solutions containing the Ste50 SAM domain did not yield any binding-induced ITC signals, indicating a lack of interactions (Figure 5C). The interaction between the L57R and the Ste50 SAM appears to be primarily entropically driven (endothermic reaction) as indicated by an upward position of the ITC peaks and positive values of the integrated heats (Figure 5B). Conversely, binding of the native Ste11 SAM with the Ste50 SAM is accompanied by the occurrence of two distinct phases. At the lower concentration ratios of the SAM domains, the interaction is characterized by the release of heat or an enthalpy-driven complex formation followed by an endothermic reaction at higher molar ratios (Figure 5A). This apparently anomalous behavior may result from the intrinsic tendency toward the formation of high molecular weight aggregates of the Ste11 SAM and Ste50 SAM heterocomplexes (*30*). Such aggregate formation was also observed between the L57R mutant and the Ste50 SAM as suggested by broad NMR resonances of the complex (data not shown). Analyses of ITC data yielded equilibrium association constants (K_a) of 97×10^8 and 85×10^{10} M^{-1} for the native Ste11 SAM and L57R mutant, respectively. The binding free energies were estimated to be −8.0 and −5.25 kcal/mol for the native Ste11 SAM and the L57R, respectively. As it appears, the mutant protein L57R binds to the Ste50 SAM with a much lower affinity as compared to the native SAM domain.

The presence of tryptophan residues only in the Ste50 SAM domain allows us to examine its interaction with the Ste11 SAM domain and the two interfacial mutants. There is a progressive quenching of the tryptophan fluorescence intensity of the Ste50 SAM on addition of the native Ste11 SAM domain (Figure 6). This result is in agreement with our previous observation carried out using a somewhat longer version of the Ste50 protein (M27−Q131) (*30*). Quenching of the tryptophan fluorescence intensity can also be seen for the L57R mutant, indicating its interactions with the Ste50 SAM (Figure 6). However, the extent of quenching was found to be much lower as compared to that of the native Ste11 SAM (Figure 6), indicating presumably a low-affinity interaction. On the other hand, no change in fluorescence of the Ste50 SAM was detected with the additions of L60R, demonstrating the inability of the mutant protein to form a heterocomplex (Figure 6).

DISCUSSION

Monomeric solution structures have been determined for many SAM domains from a variety of proteins including

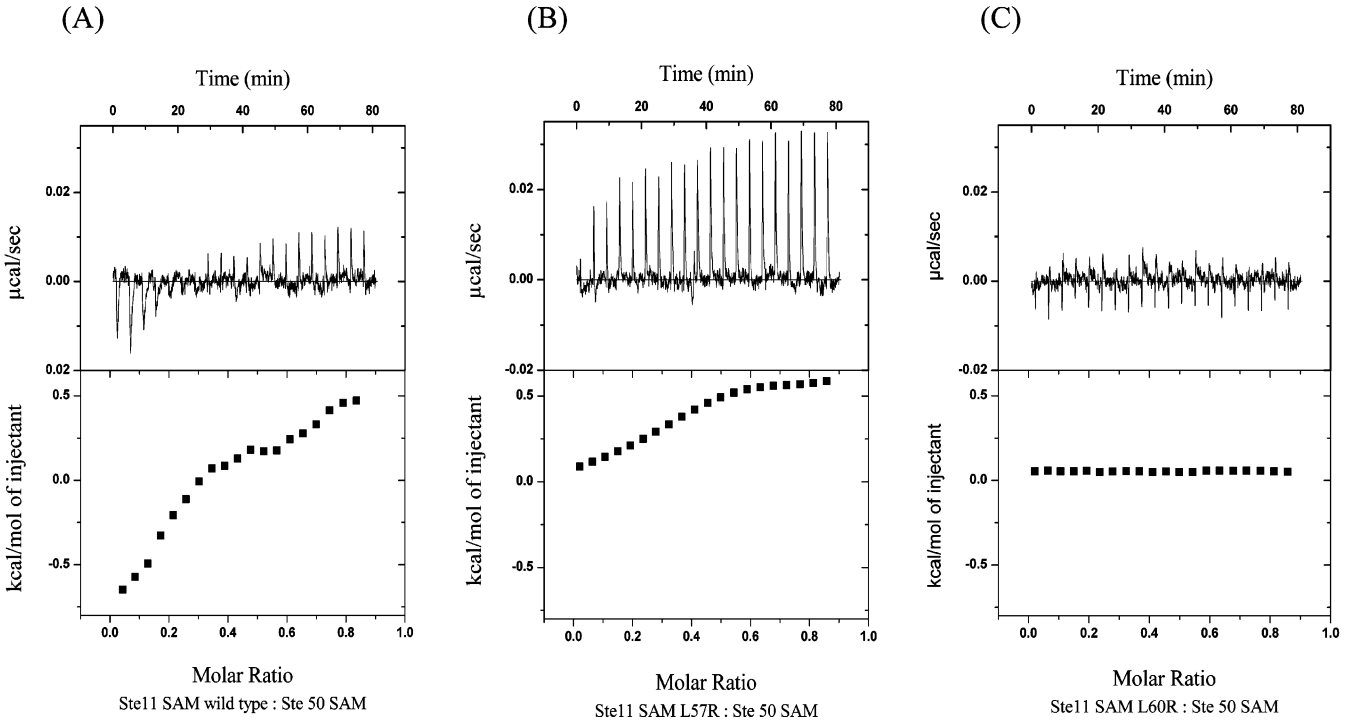

FIGURE 5: Isothermal calorimetric titrations for the interactions of the Ste50 SAM with the native Ste11 SAM (A), the L57R mutant (B), and the L60R mutant (C). Experiments were carried out by injecting 5 μL aliquots either of the native Ste11 SAM or of the two mutant proteins from a 120 μL stock into the sample cell containing the Ste50 SAM domain in 10 mM sodium phosphate buffer, 150 mM sodium chloride, and 20 mM β-mercaptoethanol, pH 6.8.

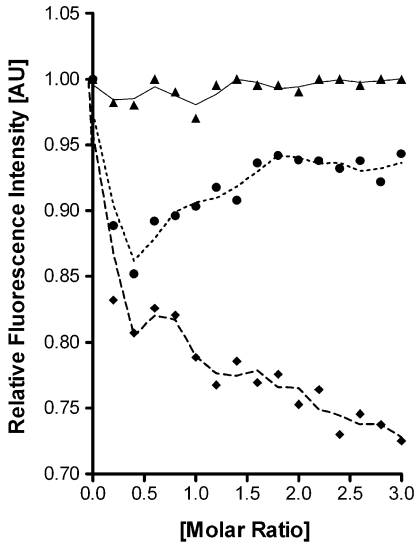

FIGURE 6: Change in the fluorescence intensity of tryptophan residues of the Ste50 SAM domain as a function of increasing concentrations of the native Ste11 SAM domain (◆) and its mutants L57R (●) and L60R (▲), respectively. Emission spectra were recorded using an excitation wavelength of 280 nm. Protein samples were prepared in 10 mM sodium phosphate buffer containing 150 mM sodium chloride and 20 mM β-mercaptoethanol at pH 6.8.

those of p73 (*22*), Ste50 (*23*, *27*), Eph B2 (*24*), Ets (*26*), and neubarin (*28*). On the other hand, polymeric structures have also been reported for other SAM domains, e.g., those of ph (*15*), Tel (*14*), Yan (*16*), Scm (*7*), and shank protein (*17*). High-resolution structures of these polymeric SAM domains could be obtained only after mutation of interfacial hydrophobic residues to charged residues to stabilize monomeric or soluble forms. A dimeric structure of the SAM domain from Eph A4 receptor kinase was realized only at higher protein concentrations (≥1 mM) (*25*). Although a folded monomeric structure was prevalent at lower concentrations, replacements of several hydrophobic residues at the dimer interface were found to favor the folded monomeric form (*25*). Interestingly, the SAM domain of the Eph B2 protein forms oligomeric structures as well as a folded monomeric structure depending on the crystal forms (*4*, *38*). The global stabilities of the native Eph B2 SAM domain and its interface mutant appear to be very similar as shown by thermal unfolding studies using CD spectroscopy (*38*). It was postulated that the oligomeric interfaces of the SAM domains, rather than playing any significant role in the structures and stabilities, may be primarily responsible for some of their functional activities (*4*, *25*). Recently, we determined a dimeric structure of the Ste11 SAM domain using NMR spectroscopy (*29*). In our study, a folded monomeric form of the Ste11 SAM domain could not be detected over the concentration range from 1 mM to 100 μM (*29*). The NMR-derived dimeric structure of the Ste11 SAM domain is uniquely organized by mutual packing among hydrophobic residues I44′, I45′, and A47′ from helix 4′ of one subunit and I53, L57, and L60 from helix 5 of the other subunit (Figure 1). These hydrophobic residues are typical of the Ste11 SAM sequence since they are not conserved among other SAM domains (*29*). A monomeric structure of the Ste11 SAM domain was also deduced from NMR data whereby many of these interfacial residues were found to be exposed to solvent (*39*).

In this current work, we have demonstrated that the urea-induced unfolding of the dimeric structure of the Ste11 SAM follows a two-state mechanism whereby only the native and the unfolded states are detected during unfolding. At intermediate concentrations of urea, i.e., 5.0−5.5 M, both the native and unfolded states were found to coexist, with

the global unfolding occurring at a 6.0 M urea concentration (Figure 2A). The unfolding of the native Ste11 SAM domain seems to be highly cooperative in that residues from different regions of the molecule are found to have similar C_m values (Figure 2B,C). A two-state thermal unfolding of the monomeric SAM domain from p73 protein was reported on the basis of studies using differential scanning calorimetry and optical spectroscopy (*40*).

Our results have shown that the hydrophobic residues in the dimeric interface are actively involved in maintaining the structural integrity and stability of the Ste11 SAM domain. The L60R mutant protein undergoes extensive aggregations as indicated by the broad HSQC resonances and size-exclusion chromatography studies (Figure 3). In the dimeric structure, residue L60 is in close proximity to L60′ from another subunit (Figure 1). Replacing the hydrophobic residue to a positively charged residue, Arg, is likely to bring ionic repulsion between the subunits that could lead to a dramatic destabilization of the interface. The extensive self-association observed for the L60R interfacial mutant is presumably occurring as a consequence of the disruption of intersubunit interactions. Such destabilization can result in an exposure of other hydrophobic residues from the interface, thereby promoting formation of soluble aggregates. The aggregated state of L60R is rich in helical structure, presumably nativelike, and extremely resistant against urea-induced unfolding (Figure 3). On the other hand, the L57R mutant protein retains the dimeric structure but unfolds at a much lower urea concentration as compared to the native Ste11 SAM domain (Figure 4). The H/D exchange studies have clearly demonstrated that the L57R mutant is significantly less stable than the native Ste11 SAM (Figure 4). The reduction in conformational stability imparted by the L57R mutation may arise from a weaker packing between R57 and I44′ and I46′ at the interface. Therefore, it appears that the interactions among nonpolar residues at the interfacial region of the Ste11 SAM are responsible for the overall stability of the folded structure. Taken together, it is likely that the Ste11 SAM domain could be a unique example of an *obligatory* dimeric SAM domain structure. The recognized binding partner of the Ste11 SAM domain is another SAM domain from the adaptor protein called Ste50 (*33*). We have previously demonstrated that interactions between these SAM domains lead to the stabilization of high molecular weight heterogeneous oligomeric structures rather than the formation of a well-defined heterocomplex (*30*). H/D exchange studies indicated residues from the interfacial region of the Ste11 SAM domain, in particular those in helix 5, may be involved in the interaction with the Ste50 SAM domain (*29*). Interestingly, mutational studies aimed to determine critical residues involved in the Ste11 SAM and Ste50 SAM interactions had identified, using surface plasmon resonance, nonpolar residues belonging to the dimer interface region of the Ste11 SAM domain (*27*, *39*). Our ITC and intrinsic tryptophan fluorescence studies delineate that the L57R mutant protein is able to interact with the Ste50 SAM domain presumably due to the preservation of the nativelike dimeric structure. A significant reduction in the binding affinity of the L57R mutant protein toward the Ste50 SAM suggests that L57 is a critical residue for binding. On the other hand, the inability of the L60R mutant to interact with the Ste50 SAM domain, observed in the present study, could be an outcome of extensive self-association, causing burial of the recognition surfaces for the Ste50 SAM domain.

The results obtained in this study may also have some functional significance. The structural integrity of the obligatory "closed" dimeric form of the Ste11 SAM domain could be important in maintaining a repressed state of the Ste11 kinase (*29*, *33*). Since yeast two-hybrid and coimmunoprecipitation experiments demonstrated that the full-length Ste11 exists in a homodimeric form (*41*, *42*), it is likely that interaction of Ste50 with the Ste11 SAM may result in opening of the interfacial residues. The exposed nonpolar residues of the Ste11 SAM domain may further stimulate the formation of high molecular weight Ste11/Ste50 heterooligomers (*30*). Interestingly, a similar mechanism of activation of signaling pathways by dynamic polymerization of protein interaction domains has recently been observed for the Wnt signaling systems (*43*). In conclusion, we have shown that unlike those of other SAM domains the conformational stability and the natively folded structure of the Ste11 SAM domain are highly dependent on the structural integrity of the dimeric interfacial region. The interface is the active moiety of the Ste11 SAM domain responsible both for binding to the cognate Ste50 and for the structural integrity of this unique SAM domain.

REFERENCES

1. Kim, C. A., and Bowie, J. U. (2003) SAM domains: uniform structure, diversity of function, *Trends Biochem. Sci. 28*, 625−628.
2. Qiao, F., and Bowie, J. U. (2005) The many faces of SAM. *Sci. STKE 286*, re7.
3. Gundelfinger, E. D., Boeckers, T. M., Baron, M. K., and Bowie, J. U. (2006) A role for zinc in postsynaptic density asSAMbly and plasticity?, *Trends Biochem. Sci. 7*, 366−373.
4. Thanos, C. D., Goodwill, K. E., and Bowie, J. U. (1999) Oligomeric structure of the human EphB2 receptor SAM domain, *Science 283*, 833−836.
5. Ponting, C. P. (1995) SAM: a novel motif in yeast sterile and Drosophila polyhomeotic proteins, *Protein Sci. 4*, 1928−1930.
6. Schultz, J., Ponting, C. P., Hofmann, K., and Bork, P. (1997) SAM as a protein interaction domain involved in developmental regulation, *Protein Sci. 6*, 249−253.
7. Kim, C. A., Sawaya, M. R., Cascio, D., Kim, W., and Bowie, J. U. (2005) Structural organization of a Sex-comb-on-midleg/polyhomeotic copolymer, *J. Biol. Chem. 280*, 27769−27775.
8. Poirel, H., Lopez, R. G., Lacronique, V., Della Valle, V., Mauchauffé, M., Berger, R., Ghysdael, J., and Bernard, O. A. (2000) Characterization of a novel ETS gene, TELB, encoding a protein structurally and functionally related to TEL, *Oncogene 19*, 4802−4806.
9. Peterson, A. J., Kyba, M., Bornemann, D., Morgan, K., Brock, H. W., and Simon, J. (1997) A domain shared by the polycomb group proteins Scm and ph mediates heterotypic and homotypic interactions, *Mol. Cell. Biol. 17*, 6683−6692.
10. Ramachander, R., Kim, C. A., Philips, M. L., Mackereth, C. D., Thanos, C. D., McIntosh, L. P., and Bowie, J. U. (2002) Oligomerization-dependent association of the SAM domains from Schizosaccharomyces pombe Byr2 and Ste4, *J. Biol. Chem. 277*, 39585−39593.
11. Hock, B., Bohme, B., Karn, T., Yamamoto, T., Kaibuchi, K., Holtrich, U., Holland, S., Pawson, T., Rubsamen-Waigmann, H., and Strebhardt, K. (1998) PDZ-domain-mediated interaction of the Eph-related receptor tyrosine kinase EphB3 and the ras-binding protein AF6 depends on the kinase activity of the receptor, *Proc. Natl. Acad. Sci. U.S.A. 95*, 9779−9784.
12. Stein, E., Lane, A. A., Cerretti, D. P., Schoecklmann, H. O., Schroff, A. D., Van Etten, R. L., and Daniel, T. O. (1998) Eph receptors discriminate specific ligand oligomers to determine alternative signaling complexes, attachment, and assembly responses, *Genes Dev. 12*, 667−678.

13. Kasten, M., and Giordano, A. (2001) Cdk10, a Cdc2-related kinase, associates with the Ets2 transcription factor and modulates its transactivation activity, *Oncogene 20*, 1832−1838.
14. Kim, A. C., Phillips, M. L., Kim, W., Gingery, M., Tran, H. H., Robinson, M. A., Faham, S., and Bowie, J. U. (2001) Polymerization of the SAM domain of TEL in leukemogenesis and transcriptional repression, *EMBO J. 20*, 4173−4182.
15. Kim, C. A., Gingery, M., Pilpa, R. M., and Bowie, J. U. (2002) The SAM domain of polyhomeotic forms a helical polymer, *Nat. Struct. Biol. 9*, 453−457.
16. Qiao, F., Song, H., Kim, C. A., Sawaya, M. R., Hunter, J. B., Gingery, M., Rebay, I., Courey, A. J., and Bowie, J. U. (2004) Derepression by depolymerization; structural insights into the regulation of Yan by Mae, *Cell 118*, 163−173.
17. Baron, M. K., Boeckers, T. M., Vaida, B., Faham, S., Gingery, M., Sawaya, M. R., Salyer, D., Gundelfinger, E. D., and Bowie, J. U. (2006) An architectural framework that may lie at the core of the post synaptic density, *Science 311*, 531−535.
18. Aviv, T., Lin, Z., Lau, S., Rendl, L. M., Sicheri, F., and Smibert, C. A. (2003) The RNA-binding SAM domain of Smaug defines a new family of post-transcriptional regulators, *Nat. Struct. Biol. 10*, 614−621.
19. Green, J. B., Gardner, C. D., Wharton, R. P., and Aggarwal, A. K. (2003) RNA recognition via the SAM domain of Smaug, *Mol. Cell 11*, 1537−1548.
20. Johnson, P. E., and Donaldson, L. W. (2006) RNA recognition by the Vts1p SAM domain, *Nat. Struct. Mol. Biol. 13*, 177−178.
21. Slupsky, C. M., Gentile, L. N., Donaldson, L. W., Mackereth, C. D., Seidel, J. J., Graves, B. J., and McIntosh, L. P. (1998) Structure of the Ets-1 pointed domain and mitogen-activated protein kinase phosphorylation site, *Proc. Natl. Acad. Sci. U.S.A. 95*, 12129−12134.
22. Chi, S. W., Ayed, A, and Arrowsmith, C. H. (1999) Solution structure of a conserved C-terminal domain of p73 with structural homology to the SAM domain, *EMBO J. 18*, 4438−4445.
23. Grimshaw, S. J., Mott, H. R., Stott, K. M., Nielson, P. R., Evetts, K. A., Hopkins, L. J., Nietlispach, D., and Owen, D. (2004) Structure of the SAM domain of the *S. cerevisiae* MAPK pathway modulating protein STE50 and analysis of its interaction with STE11 SAM, *J. Biol. Chem. 279*, 2192−2201.
24. Smalla, M., Schmieder, P., Kelly, M., Ter-Laak, A., Krause, G., Ball, L., Wahl, M., Bork, P., and Oschkinat, H. (1999) Solution structure of the receptor tyrosine kinase EphB2 SAM domain and identification of two distinct homotypic interaction sites, *Protein Sci. 8*, 1954−1961.
25. Stapleton, D., Balan, I., Pawson, T., and Sicheri, F. (1999) The crystal structure of an Eph receptor SAM domain reveals a mechanism for modular dimerization, *Nat. Struct. Biol. 6*, 44−49.
26. Mackereth, C. D., Schärpf, M., Gentile, L. N., MacIntosh, S. E., Slupsky, C. M., and McIntosh, L. P. (2004) Diversity in structure and function of the Ets family PNT domains, *J. Mol. Biol. 342*, 1249−1264.
27. Kwan, J. J., Warner, N., Maini, J., Chan, Tung, K. W., Zakaria, H., Pawson, T., and Donaldson, L. W. (2006) Saccharomyces cerevisiae Ste50 binds the MAPKKK Ste11 through a head-to-tail SAM domain interaction, *J. Mol. Biol. 356*, 142−154.
28. Ju, T., Ragusa, M. J., Hudak, J., Nairn, A. C., and Peti, W. (2007) Structural characterization of the neurabin sterile alpha motif domain, *Proteins 69*, 192−198.
29. Bhattacharjya, S., Xu, P., Gingras, R., Shaykhutdinov, R., Wu, C., Whiteway, M., and Ni, F. (2004) Solution structure of the dimeric SAM domain of MAPKKK Ste11 and its interactions with the adaptor protein Ste50 from the budding yeast: implications for Ste11 activation and signal transmission through the Ste50-Ste11 complex, *J. Mol. Biol. 344*, 1071−1087.
30. Bhattacharjya, S., Xu, P., Chakrapani, M., Johnston, L., and Ni, F. (2005) Polymerization of the SAM domain of MAPKKK Ste11 from the budding yeast: implications for efficient signaling through the MAPK cascades, *Protein Sci. 14*, 828−835.
31. Bhattacharjya, S., Gingras, R., and Xu, P. (2006) An NMR-based identification of a peptide fragment from the beta-subunit of a G-protein showing specific interactions with the GBB domain of the Ste20 kinase in budding yeast, *Biochem. Biophys. Res. Commun. 347*, 1145−1150.
32. Stevenson, B. J., Rhodes, N., Errede, B., and Sprague, G. Jr. (1992) Constitutive mutants of the protein kinase STE11 activate the yeast pheromone response pathway in the absence of the G protein, *Genes Dev. 6*, 1293−1304.
33. Wu, C., Leberer, E., Thomas, D. Y., and Whiteway, M. (1999) Functional characterization of the interaction of Ste50p with Ste11p MAPKKK in *Saccharomyces cerevisiae*, *Mol. Biol. Cell 10*, 2425−2440.
34. Delaglio, F., Grzesiek, S., Vuister, G. W., Zhu, G., Pfeifer, J., and Bax, A. (1995) NMRPipe: a multidimensional spectral processing system based on UNIX pipes, *J. Biomol. NMR 4*, 603−614.
35. Johnson, B. A., and Blevins, R. A. (1994) NMRVIEW: a computer program for the visualization and analysis of NMR data, *J. Biomol. NMR 6*, 277−293.
36. Van Mierlo, C., Van der Oever, J., and Steensma, E. (2000) Apoflavodoxin (un)folding at residue level by NMR, *Protein Sci. 9*, 145−157.
37. Bai, Y., Milne, J. S., Mayne, L., and Englander, S. W. (1993) Primary structure effects on peptide group hydrogen exchange, *Proteins 17*, 75−86.
38. Thanos, C. D., Faham, S., Goodwill, K. E., Cascio, D., Phillips, M., and Bowie, J. U. (1999) Monomeric structure of the human EphB2 sterile alpha motif domain, *J. Biol. Chem. 274*, 37301−37306.
39. Kwan, J. J., Warner, N., Pawson, T., and Donaldson, L. W. (2004) The solution structure of the S.cerevisiae Ste11 MAPKKK SAM domain and its partnership with Ste50, *J. Mol. Biol. 342*, 681−693.
40. Barrera, F. N., Garzón, M. T., Gómez, J., and Neira, J. L. (2002) Equilibrium unfolding of the C-terminal SAM domain of p73, *Biochemistry 41*, 5743−5753.
41. Barr, M. M., Tu, H., Van Aelst, L., and Wigler, M. (1996) Identification of Ste4 as a potential regulator of Byr2 in the sexual response pathway of *Schizosaccharomyces pombe*, *Mol. Cell. Biol. 16*, 5597−5603.
42. Ramezani-Rad, M., Jansen, G., Buhring, F., and Hollenberg, C. P. (1998) Ste50p is involved in regulating filamentous growth in the yeast *Saccharomyces cerevisiae* and associates with Ste11p, *Mol. Gen. Genet. 259*, 29−38.
43. Schwarz-Romond, T., Fiedler, M., Shibata, N., Butler, P. J., Kikuchi, A., Higuchi, Y., and Bienz, M. (2007) The DIX domain of dishelleved confers Wnt signaling by dynamic polymerization, *Nat. Struct. Mol. Biol. 6*, 484−492.

BI701941Z